Appl Petrochem Res (2017) 7:97–105
https://doi.org/10.1007/s13203-017-0181-6

ORIGINAL ARTICLE

Improved performance of hierarchical porous Mo/H-IM-5 catalyst in methane non-oxidative aromatization

Heng Liu[1] · **Qiubin Kan**[2]

Received: 22 September 2016 / Accepted: 7 September 2017 / Published online: 18 September 2017

Abstract Two novel hierarchical porous IM-5-S and IM-5-M materials were synthesized using mesoporous silica SBA-15 and MCM-48 as the silica sources, and for comparison conventional IM-5-C zeolite was also synthesized with the same synthesis composition. IM-5-S and IM-5-M samples exhibited larger crystal sizes and different textural properties than the conventional IM-5-C zeolite. Moreover, Mo-modified catalysts, Mo-IM-5-S, Mo-IM-5-M, and Mo-IM-5-C, were prepared for the non-oxidative aromatization of methane. The physical properties and acidities of the samples were characterized by XRD, SEM, TEM, BET, and NH_3-TPD. Compared with Mo-IM-5-C, the Mo-IM-5-S and Mo-IM-5-M catalysts showed higher yields of aromatics and better stabilities. The preferable catalytic behaviors of Mo-modified mesoporous IM-5 catalysts may be attributed to the generation of secondary mesoporous systems within the zeolite crystals, which may influence the location and state of the active Mo species, simultaneously lead to easier access to the active sites for reactants and be favorable for the diffusion of products formed in the microporous channels during the methane aromatization reaction.

Keywords Mesoporous · IM-5 · Zeolite · Molybdenum · Methane aromatization

✉ Heng Liu
liuhengjlu@163.com

[1] Research Center for Nanotechnology, Changchun University of Science and Technology, Changchun 130022, People's Republic of China

[2] College of Chemistry, Jilin University, Changchun 130023, People's Republic of China

Introduction

With the gradual depletion of world petroleum resources, it is becoming increasingly important for efficient use of natural gas. As the most abundant component in natural gas, methane is currently suggested as an alternative source for producing liquid fuels and valuable chemicals [1]. In 1993, Wang et al. reported a highly active catalyst, Mo/HZSM-5, for methane dehydroaromatization (MDA) under non-oxidative conditions [2]. Since then, many researchers have worked on this significant catalytic process and made encouraging progress. Different types of molecular sieves have been investigated, and zeolite such as ZSM-5 has been confirmed to be suitable support for methane non-oxidative aromatization [3–6]. Moreover, different metal species (Mo, Fe, Zn, W, Re, Cu, Mn, Ni, Cr, V, Ga, etc.) have been evaluated as the active sites of the catalysts [7–10]. Mo-modified catalysts exhibit the highest activity in the conversion of methane to aromatics. Catalysts modified by W, Re, and Co–Ga species also perform well, while other metal species exhibit low activity for methane aromatization. However, catalyst deactivation due to the rapid deposition of polyaromatics and coke is a major obstacle to commercialization for the title reaction [11, 12]. Various strategies, focused on optimization of the zeolite supports and addition of the promoters, have been tested to improve the catalytic activity and stability of the catalysts. It has been found that dealumination, external surface silanation, post-synthesis hydrothermal treatment, addition of second metal component, etc., are effective ways to improve the performance of the catalysts [13–15]. In recent studies, Zhang investigated the performance of eight kinds of transition metal-modified Mo/HZSM-5 catalysts in MDA with periodic CH_4–H_2 switching [16]. Bao et al. reported that single iron sites embedded in a silica matrix

can catalytically convert methane to ethylene and aromatics under non-oxidative conditions directly, and the lattice-confined single iron sites exhibited high stability during a 60-h test [17].

Recently, the catalytic behaviors of IM-5 zeolite in shape-selective catalysis, xylene isomerization–disproportionation, hydrocarbon cracking, and selective catalytic reduction of nitric oxides have been investigated [18–21]. Moreover, the creation of a proper mesoporosity in the zeolite system has been achieved through various ways, such as the post-treatment method and the template method. Extending the application of hierarchical porous materials has been considered significant [22–25]. According to this direction, in this paper, hierarchical porous IM-5-S and IM-5-M were synthesized using mesoporous materials SBA-15 and MCM-48 as the silica sources. Mo-modified mesoporous Mo-IM-5-S and Mo-IM-5-M catalysts were prepared and tested for MDA reaction. For comparison, the performance of conventional Mo-IM-5-C catalyst was also studied.

Experimental

Catalyst preparation

In the synthesis process, ordered mesoporous materials SBA-15 and MCM-48 were synthesized first. For the synthesis of SBA-15, triblock polymer P123 was dissolved in the deionized water and HCl solution with stirring at 313 K. Then, the required amount of TEOS was added to that solution and the mixture was stirred at 313 K for 6 h. The molar composition of the mixture was 0.017 P123:SiO_2:6 HCl:192 H_2O. The mixture was heated to 373 K in an oven for 24 h. For the synthesis of MCM-48, cetyltrimethylammonium bromide (CTAB) and NaOH were added to the deionized water solution with stirring for 1 h. Then, the required amount of TEOS was added to that solution and the mixture was stirred for 2 h. The molar composition of the mixture was 0.59 CTAB:TEOS:0.5 NaOH:61 H_2O. The mixture was transferred to an autoclave and the reaction was carried out at 383 K for 72 h. After crystallization, the solids were filtered, washed with deionized water, and dried in air at room temperature. The samples were calcined in air at 823 K for 6 h and the white powder SBA-15 and MCM-48 were obtained.

For the synthesis of mesoporous IM-5-S and IM-5-M, the calcined SBA-15 and MCM-48 were added into the synthesis system as the silica sources. The procedure is described as follows: the structure-directing agent 1,5-bis(methylpyrrolidinium)pentane (1,5-MPP) and the required amount of SBA-15 or MCM-48 were mixed in 30 mL water. Then, sodium hydroxide and aluminum nitrate nonahydrate were added to the solution with vigorous stirring for 24 h. The chemical composition of the synthesis system was 30 SiO_2: 4.5(1,5-MPP): 0.6 Al_2O_3: 11 Na_2O: 1200 H_2O. The mixtures were crystallized in Teflon-lined autoclaves under rotating condition (continuous stirring at 60 rpm) at 433 K for 10 days. The solid was obtained after filtration, washed with distilled water, and dried overnight at 373 K. To prepare the calcined IM-5-S and IM-5-M, the organic templates were burned away through heating the samples at 823 K for 6 h. After repeating the ion exchange of the calcined IM-5-S and IM-5-M two times with a 1 mol/L solution of ammonium nitrate at 363 K and calcination of the products in air at 773 K for 5 h, H-IM-5-S and H-IM-5-M were obtained. Then, H-IM-5-S and H-IM-5-M were physically mixed with 6 wt% MoO_3 and calcined in air at 773 K for 3 h as described in Ref. [13]. Mo-modified samples are denoted as Mo-IM-5-S and Mo-IM-5-M. The MoO_3 species content in the catalyst was measured by chemical analysis.

Following the same procedure described above, conventional IM-5 zeolite (IM-5-C) was synthesized using fumed silica as the silica source [21]. Conventional Mo-modified Mo-IM-5-C catalyst was also prepared for the MDA reaction.

Characterization

The samples were characterized by X-ray diffraction (XRD) on the SHIMADZU XRD-6000 diffractometer with CuKα radiation in the 2θ angle ranging from 5° to 40°. The field emission scanning electron microscope (FESEM) XL-30 was carried out to observe the morphology of the products. The transmission electron microscope (TEM) images were obtained using JEOL JEM-1200EX electron microscope with an accelerating voltage of 100 kV. The element contents were analyzed by a Perkin-Elmer inductively coupled plasma atomic emission spectroscopy (ICP-AES). Nitrogen adsorption analyses were tested with a Micromeritics ASAP 2020 system at 77 K. The product was degased at 523 K for 3 h prior to the measurements. The Brunauer–Emmett–Teller (BET) method and t plot analysis were used to obtain the BET surface area and the average pore volume of the sample. Temperature-programmed desorption of NH_3 (NH_3-TPD) was carried out on a conventional system rigged with a thermal conductivity detector. Thermogravimetric analysis (TGA) was performed using a Shimadzu DTG-60.

Catalytic evaluation

The reaction of methane aromatization was tested under atmospheric pressure in a fixed-bed quartz reactor (10 mm i.d.) at 973 K, and 0.5 g of the sample pelleted at 40–60

mesh size was charged into the reactor. The feed gas (92.5% CH_4 and 7.5% N_2) was added into the reactor through a mass flow controller at 1500 mL/g h. An online gas chromatograph (Shimadzu GC-17A) rigged with a 6 m × 3 mm HayeSep D 80/100 column and an online TCD detector were used to measure N_2, H_2, CO, CH_4, C_2H_4, and C_2H_6. A CBP1-M50-025 (Shimadzu) quartz capillary column and an online FID detector were used to measure the aromatic products of benzene, toluene, and naphthalene. The conversion of methane and the selectivity of aromatic and hydrocarbon products were calculated according to the carbon mass balance using an N_2 internal standard method [14].

Results and discussion

XRD studies

Figure 1 exhibits the small angle XRD patterns of SBA-15 and MCM-48. The XRD patterns showed the characteristic diffraction peaks as described in the literature [26, 27], indicating that the well-ordered mesoporous SBA-15 and MCM-48 materials were successfully synthesized. The high angle XRD patterns of IM-5-S, IM-5-M, and IM-5-C are also shown in Fig. 1. The patterns exhibited the same characteristics as described in Ref. [18], which indicated that using mesoporous silica SBA-15 and MCM-48 as the silica sources in the synthesis gels did not affect the formation of well-ordered IM-5 zeolites. Although the crystallinity of the IM-5 samples reduced after the physical mixing process, the framework of zeolites was retained. The Mo-modified zeolites showed similar XRD patterns to the parent IM-5.

SEM and TEM characterization

Figure 2 exhibits the SEM and TEM images of the samples. The SEM micrograph clearly indicates that the IM-5-C zeolite was synthesized as cubical shape crystals, which is in accordance with Ref. [21]. The IM-5-S and IM-5-M zeolites were in the form of larger cubical shape crystals than the IM-5-C zeolite. Moreover, no amorphous material was found in the three samples, proving that the IM-5-C, IM-5-S, and IM-5-M zeolites had a high crystallinity. The crystal morphologies of the three samples were almost retained after modification of the MoO_3 species. The TEM images showed that the crystal size of conventional IM-5-C was around 500 nm, and the crystal size of mesoporous IM-5-S and IM-5-M was in the range of 500–1000 and 1000–2000 nm, respectively. Furthermore, the crystals of IM-5-S and IM-5-M displayed some bright lines and bright spots in the white circles of the TEM images, which were not observed in the image of conventional IM-5-C. These bright fields may be relative to the formation of intracrystal mesopores. It is supposed that mesopores were formed following a series of dissolution, self-assembly, nucleation, and crystallization processes. The intracrystal pores were different from the regular mesopore structures of SBA-15 and MCM-48 materials and were randomly distributed in the whole crystals. The SEM and TEM images proved that using mesoporous silica SBA-15 and MCM-48 as the silica sources could generate IM-5 zeolites with larger crystal sizes and a certain amount of mesopores.

N_2 adsorption–desorption study

Figure 3 shows the N_2 adsorption–desorption isotherms and pore size distributions of IM-5-S, IM-5-M, and IM-

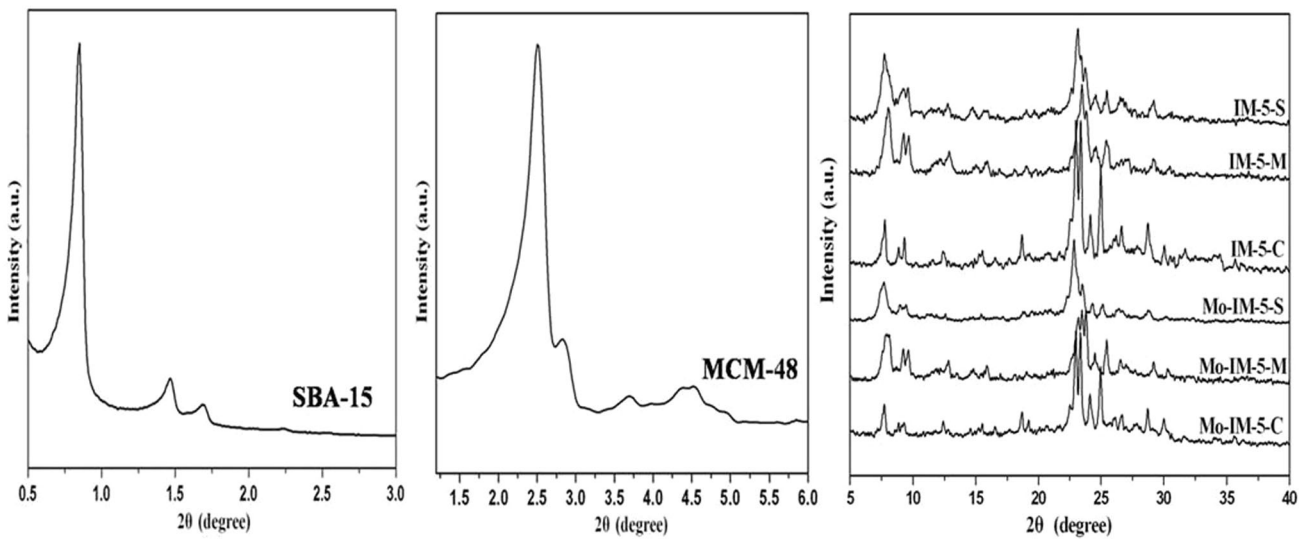

Fig. 1 The XRD patterns of SBA-15, MCM-48, IM-5-S, IM-5-M, IM-5-C, Mo-IM-5-S, Mo-IM-5-M, and Mo-IM-5-C samples

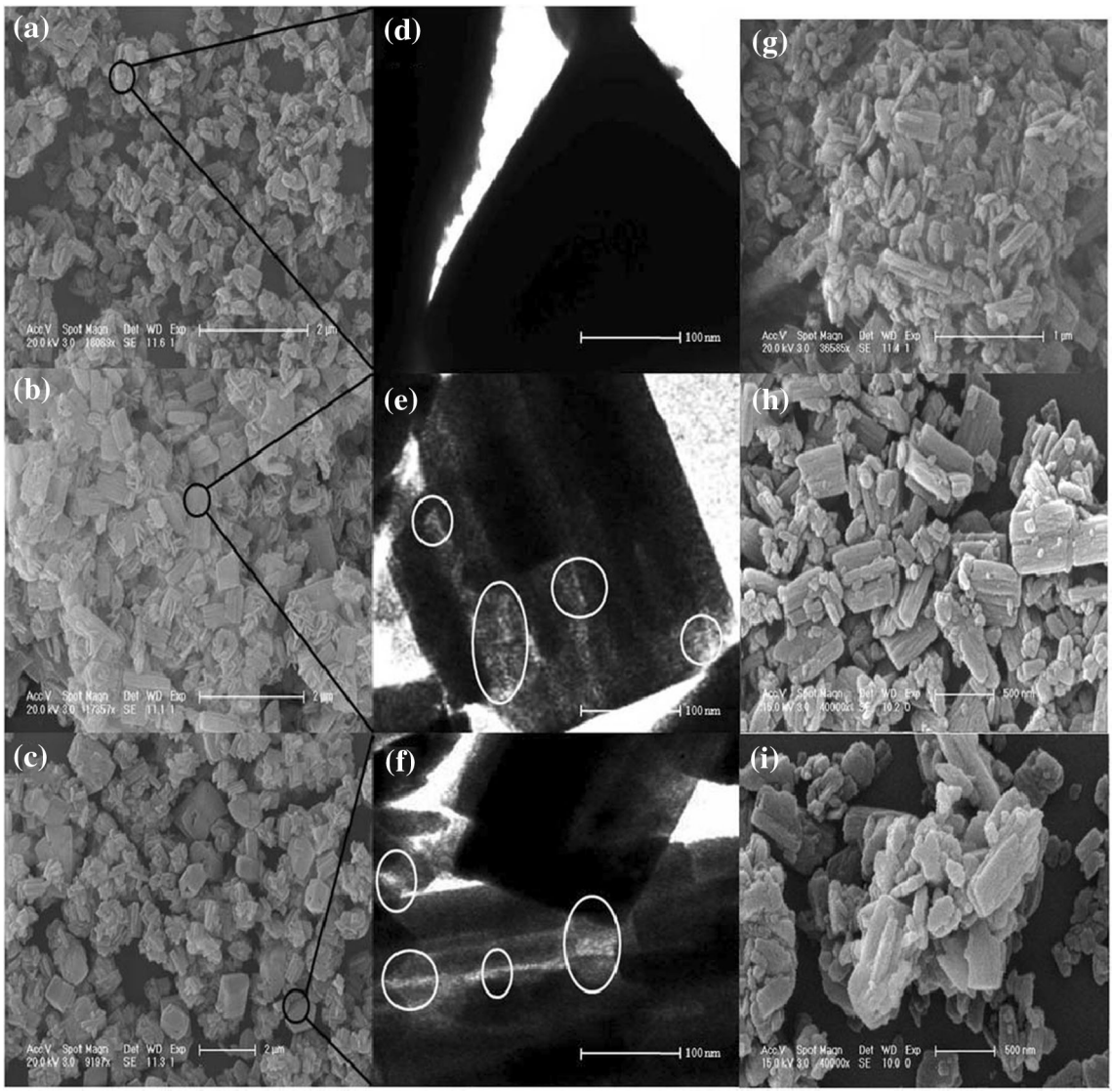

Fig. 2 The SEM images of samples **a** IM-5-C; **b** IM-5-S; **c** IM-5-M; the TEM images of samples **d** IM-5-C; **e** IM-5-S; **f** IM-5-M; and the SEM images of samples **g** Mo-IM-5-C; **h** Mo-IM-5-S; **i** Mo-IM-5-M

5-C. The patterns of the IM-5-S and IM-5-M samples displayed a hysteresis loop from $P/P_0 = 0.4$ to $P/P_0 = 1$, which may due to the N_2 adsorption and capillary condensation in the mesopores. This kind of hysteresis loop was not observed in the pattern of IM-5-C sample. The results indicated that some mesopores were generated in IM-5-S and IM-5-M samples using SBA-15 and MCM-48 as the silica sources in the synthesis system. The micropore sizes of the three samples obtained from Horvath–Kawazoe report were concentrated at 0.48 nm. As shown in Fig. 3b, c, the mesopore size of the IM-5-S sample was distributed in a wide range and concentrated in 10–20 nm, and the mesopore size of the IM-5-M sample was widely distributed and concentrated in 30–60 nm.

The Si/Al ratios, BET surface areas (S_{BET}), microporous surface areas (S_{micro}), microporous volumes (V_{micro}), mesoporous volumes (V_{meso}), and total volumes (V_{total}) of the IM-5-S, IM-5-M, and IM-5-C samples are summarized in Table 1. The Si/Al ratios of IM-5-S and IM-5-M samples were similar to that of IM-5-C. IM-5-S and IM-5-M samples showed larger total volumes and mesoporous volumes than IM-5-C. The differences in pore volumes of the three samples may be due to the formation of mesopores in IM-5-S and IM-5-M. The BET surface areas of IM-5-S and IM-5-M were 376 and 384 m^2/g, which were larger than that of IM-5-C (363 m^2/g). The generation of mesopores in IM-5-S and IM-5-M samples was accompanied by the reduction of microporous characters. IM-5-S and IM-5-M samples showed lower microporous surface

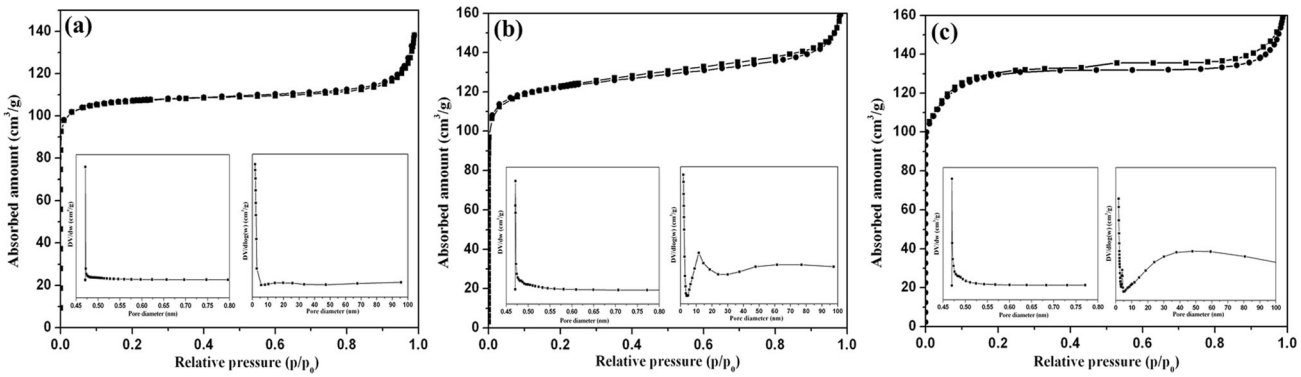

Fig. 3 The N_2 adsorption–desorption isotherms and pore size distributions of **a** IM-5-C, **b** IM-5-S, and **c** IM-5-M

Table 1 The textural properties of IM-5-C, IM-5-S, IM-5-M, Mo-IM-5-C, Mo-IM-5-S, and Mo-IM-5-M

Samples	Si/Al ratio	S_{BET} (m^2/g)	S_{micro} (m^2/g)	V_{micro} (cm^3/g)	V_{meso} (cm^3/g)	V_{total} (cm^3/g)
IM-5-C	23	363	319	0.15	0.05	0.20
IM-5-S	26	376	293	0.12	0.13	0.25
IM-5-M	25	384	286	0.11	0.16	0.27
Mo-IM-5-C	–	312	280	0.13	0.04	0.17
Mo-IM-5-S	–	321	262	0.11	0.11	0.22
Mo-IM-5-M	–	325	259	0.10	0.13	0.23

areas and microporous volumes than IM-5-C. The mesoporous IM-5 and conventional IM-5 exhibited different pore properties, which may be due to using different silica materials as the silica sources, thus influencing the formation of crystals. Moreover, the numerical results of the structural property decreased after the physical mixing process, indicating that MoO_3 were diffused in/on the zeolites.

Acidity test

The results of NH_3-TPD for H-IM-5-S, 6Mo-IM-5-S, H-IM-5-M, 6Mo-IM-5-M, H-IM-5-C, and 6Mo-IM-5-C are shown in Fig. 4. Two peaks, denoted as peak *L* and peak *H*, were observed in the NH_3-TPD graphs for H-IM-5-S, H-IM-5-M, and H-IM-5-C samples at around 480 and 680 K, which was similar to the ZSM-5 zeolite [28]. The peak at 480 K was assigned to desorption of the adsorbed NH_3 on weak acid sites, whereas the peak at 680 K was assigned to desorption of the adsorbed NH_3 to strong Brønsted acid sites. For mesoporous H-IM-5-S and H-IM-5-M, the intensities of low-temperature desorption peak were similar to that of conventional H-IM-5-C. However, the intensities of high-temperature desorption peak for H-IM-5-S and H-IM-5-M were weaker than that for conventional H-IM-5-C, which suggested that the strong acid

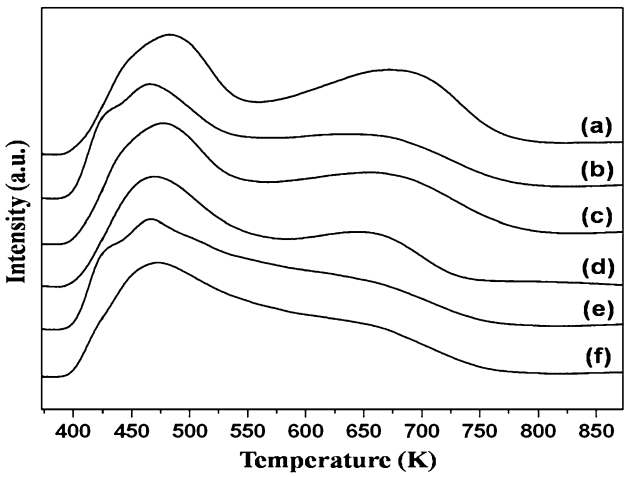

Fig. 4 The NH_3-TPD profiles of the samples: **a** H-IM-5-C, **b** H-IM-5-S, **c** H-IM-5-M, **d** Mo-IM-5-C, **e** Mo-IM-5-S, and **f** Mo-IM-5-M

capacities of the mesoporous H-IM-5-S and H-IM-5-M samples were lower than that of conventional H-IM-5-C. The peak areas at low temperature (about 486 K) and high temperature (about 683 K) for the three samples decreased with the addition of MoO_3 species, and the peak areas at high temperature decreased more sharply. Moreover, a new peak (denoted as peak *M*) appeared at around 580 K after loading of 6% MoO_3.

Table 2 The acidity capacities of H-IM-5-C, Mo-IM-5-C, H-IM-5-S, Mo-IM-5-S, H-IM-5-M, and Mo-IM-5-M

Samples	Contents of MoO_3 (wt%)	Peak (*L*) Area (a.u.)	Peak (*M*) Area (a.u.)	Peak (*H*) Area (a.u.)
H-IM-5-C	–	431	–	534
Mo-IM-5-C	5.4	375	225	281
H-IM-5-S	–	377	–	365
Mo-IM-5-S	5.4	342	188	161
H-IM-5-M	–	390	–	393
Mo-IM-5-M	5.5	359	193	179

The Gauss curve fitting method was used to analyze the NH_3-TPD profiles as described in Ref. [13]. The numerical results of acid capacities for H-IM-5-C, Mo-IM-5-C, H-IM-5-S, Mo-IM-5-S, H-IM-5-M, Mo-IM-5-M, and the contents of MoO_3 are listed in Table 2. The areas of peak H for H-IM-5-S and H-IM-5-M decreased from 365 to 161 (55.9%) and from 393 to 179 (54.5%) after modification of MoO_3, respectively. At the same time, the area of peak H for H-IM-5-C decreased from 534 to 281 (47.4%) after modification of MoO_3. Mo oxide species that interacted with the internal Brønsted acid sites play an important role in methane aromatization and are accompanied by the reduction of Brønsted acid sites [21, 28]. It can be summarized from the acidity test that a majority of MoO_3 migrated into the channels of zeolites and related to the strong Brønsted acid during the physical mixing process of MoO_3. In addition, a new peak M emerged at ca. 580 K after modification of MoO_3, and this indicated that the medium-strength acid sites were generated when the Mo species interacted with the Brønsted acid sites.

Catalytic test

The catalytic behavior of Mo-IM-5-S, Mo-IM-5-M, and Mo-IM-5-C catalysts in methane aromatization is shown in Fig. 5. The numerical results are listed in Table 3. In the initial period of the reaction, the methane conversions and aromatic yields of the three catalysts increased rapidly and achieved a maximum in 60 min. The highest conversions of methane and yields of aromatics over Mo-IM-5-S, Mo-IM-5-M, and Mo-IM-5-C were 11.8, 11.5, 11.6 and 6.3, 6.3, 6.2%, respectively (see Table 3). The three samples had similar initial conversions of methane. Afterward, the values reduced with time on stream and remained relatively stable at the later stage. As shown in Fig. 5, the Mo-IM-5-C catalyst possessed a faster rate of deactivation than the Mo-IM-5-S, and Mo-IM-5-M catalysts. When the reaction time was 420 min, the conversions of methane and yields of aromatics over Mo-IM-5-M, Mo-IM-5-S, and Mo-IM-5-C were 8.0, 8.2, 7.4 and 5.1, 5.2, 4.2%, respectively. Throughout the whole reaction process, compared with Mo-IM-5-C, Mo-IM-5-S and Mo-IM-5-M samples exhibited higher conversions of methane, yields of aromatics, and better stabilities. The catalytic performance of Mo-IM-5-S and Mo-IM-5-M in this work was also superior to the behavior of conventional Mo-IM-5 in a previous study [4]. Figure 5 also exhibits the benzene and naphthalene yields over the three catalysts. The selectivities of benzene, toluene, naphthalene, and coke are summarized in Table 3. The Mo-IM-5-M and Mo-IM-5-S catalysts displayed higher yields of benzene and naphthalene than Mo-IM-5-C. At the same time, the aromatic selectivities of Mo-IM-5-M and Mo-IM-5-S catalysts were also higher than those of Mo-IM-5-C. Moreover, the Mo-IM-5-M and Mo-IM-5-S catalysts performed lower coke selectivities than the conventional Mo-IM-5-C catalyst. The better catalytic behavior of mesoporous Mo-IM-5-S and Mo-IM-5-M can be attributed to the preferable channel structures. In this paper, two novel hierarchical IM-5-S and IM-5-M materials were synthesized using mesoporous silica SBA-15 and MCM-48 as the silica sources. After calcination of the samples, a few secondary mesopores were generated in IM-5-M and IM-5-S. The microporous structures, the shape selectivity, and long-range diffusion characteristics of zeolite were still retained in the mesoporous IM-5-M and IM-5-S samples. The existence of secondary mesoporous structures may lead to preferable access to the active sites for reactants and better diffusion of aromatic products, thus enhancing the behavior of the catalysts in the MDA reaction. Moreover, the distribution of acid sites in IM-5 zeolites can be influenced by the appearance of secondary mesoporous structures; as shown in the acidity test (Fig. 4; Table 2), the acidic strength and density then change along with it. These changes can also impact the state and location of the active Mo species. It is indicated that Mo species of the mesoporous IM-5 samples prefer to migrate into the channels associated with the internal Brønsted acid sites. In addition, Mo oxide species related to the internal Brønsted acid sites play significant roles in MDA reaction, and increasing the Mo species amount inside the channels of the support with equal Mo loading is beneficial for the generation of benzene [28]. The appropriate distribution of

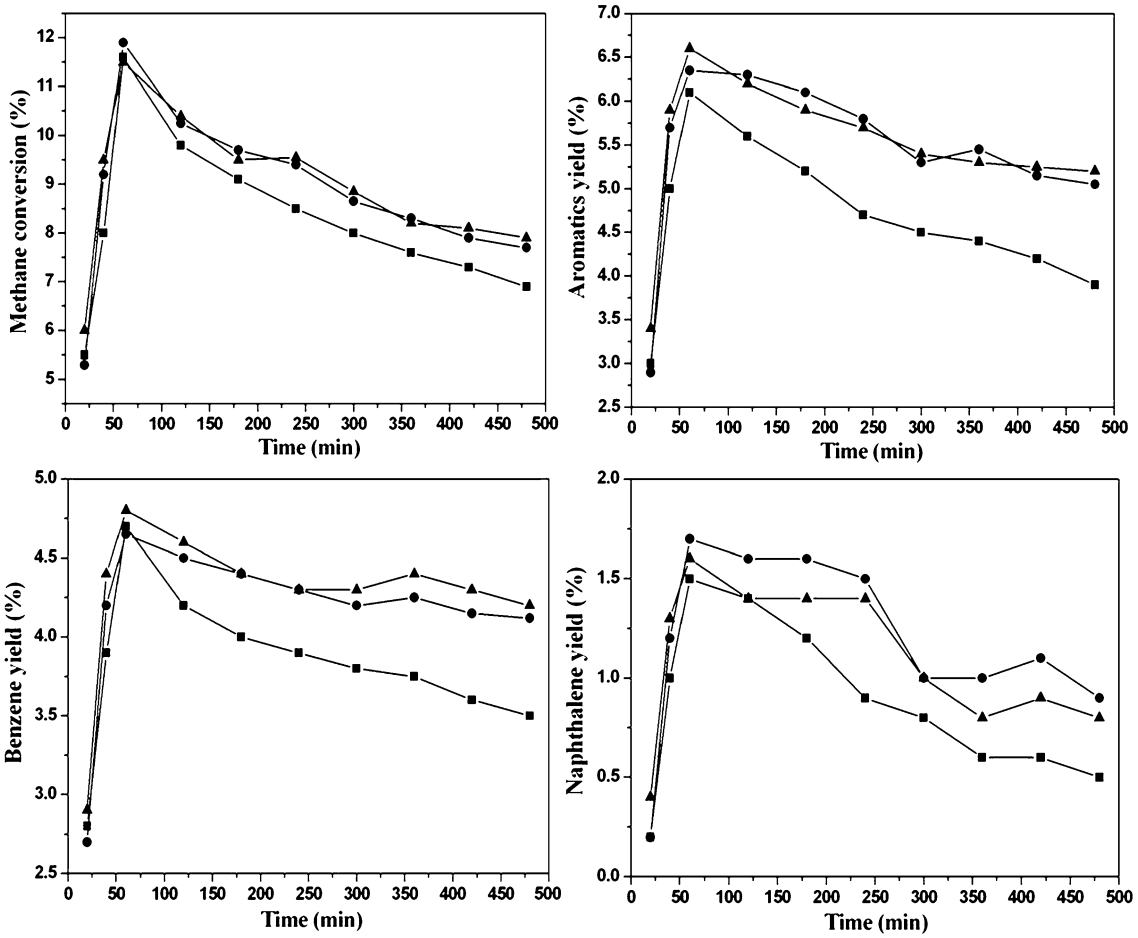

Fig. 5 The methane conversions, aromatic yields, benzene yields, and naphthalene yields over Mo-IM-5-C (filled squares), Mo-IM-5-S (filled circles), and Mo-IM-5-M (filled triangles) catalysts. Reaction condition: $T = 973$ K, 1 atm, GHSV = 1500/h

Table 3 The reaction results of methane aromatization over Mo-IM-5-C, Mo-IM-5-S and Mo-IM-5-M catalysts at 60 and 420 min

Catalysts	Reaction time (min)	Conversion of CH_4 (%)	Selectivity (%)				Aromatic yields (%)
			Benzene	Toluene	Naphthalene	Coke	
Mo-IM-5-C	60	11.6	40.5	1.3	13.1	45.1	6.2
	420	7.4	48.7	0.9	8.1	42.3	4.2
Mo-IM-5-S	60	11.8	39.6	2.2	14.6	43.6	6.3
	420	8.0	51.3	2.1	13.7	32.9	5.1
Mo-IM-5-M	60	11.5	41.7	1.9	14.1	42.3	6.3
	420	8.2	52.4	2.3	12.2	33.1	5.2

Reaction condition: $T = 973$ K, 1 atm, GHSV = 1500/h

acid sites and location of active Mo species could promote the formation of aromatic products and improve the performance of the Mo-IM-5-S and Mo-IM-5-M catalysts.

The TG analysis is carried out to determine the amount of coke after reaction for 500 min. As shown in Fig. 6, the evaporation of chemisorbed and physisorbed water led to weight loss from 300 to 500 K. Weight loss at 700–1000 K was related to the decomposition of coke. The percent of coke on the conventional Mo-IM-5-C catalyst was 8.4%, which was higher than that on mesoporous Mo-IM-5-S (7.3%) and Mo-IM-5-M (7.1%) catalysts. The selectivity of coke for Mo-IM-5-C was also higher than that for Mo-IM-5-M and Mo-IM-5-S (see Table 3). As reported in the references, deactivation of

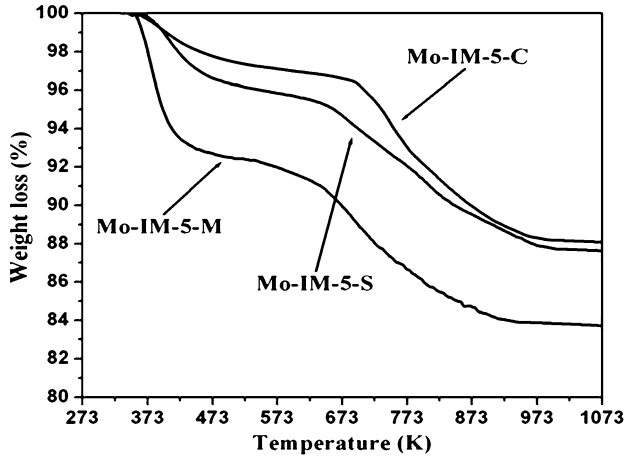

Fig. 6 The TG profiles of Mo-IM-5-C, Mo-IM-5-S, and Mo-IM-5-M samples after reaction for 500 min

the catalyst during the MDA reaction may be due to the rapid deposition of polyaromatics and coke in/on the zeolite. The Brønsted acid sites and zeolite channels could be covered and blocked by coke step by step, thus leading to the separation of active sites and reactants [11, 12]. Therefore, different amounts of coke generated in/on the samples during the MDA reaction may result in different stabilities of the catalysts. For Mo-IM-5-M and Mo-IM-5-S, it can be considered that the aromatic products, which were generated during the course of reaction, could move out of the channels timely and effectively owing to the appearance of mesopores in the zeolite. In this case, the opportunity for the generation of coke could be reduced, thus leading to the enhancement of catalyst stabilities and aromatic selectivities.

As shown in Fig. 7, the recycling experiments were carried out to investigate the long-term stabilities of the Mo-IM-5-S and Mo-IM-5-M samples. The catalysts were regenerated by calcination under air at 773 K for 3 h. It is shown that the methane conversion of Mo-IM-5-S sample for four successive runs was 11.8, 11.3, 11.5, and 11.1% after reaction for 60 min, respectively. The corresponding yield of aromatics was 6.3, 5.9, 6.2, and 5.8%. The methane conversion of Mo-IM-5-M sample for four successive runs was 11.5, 11.9, 11.2, and 10.8% after reaction for 60 min, respectively. The corresponding yield of aromatics was 6.3, 6.5, 6.2, and 5.8%. It is evident that the catalysts can be reused after being calcined to remove coke, and the mesoporous Mo-IM-5-S and Mo-IM-5-M samples show excellent stabilities.

Conclusions

Two novel hierarchical porous IM-5-S and IM-5-M zeolites have been synthesized using mesoporous silica SBA-15 and MCM-48 as the silica sources, Mo-modified catalysts of Mo-IM-5-S, Mo-IM-5-M, and conventional Mo-IM-5-C were prepared and tested for the methane dehydroaromatization reaction under non-oxidative condition at 973 K. It appears that hierarchical porous Mo-IM-5-S and Mo-IM-5-M catalysts showed higher aromatic yields and better stabilities than the Mo-IM-5-C catalyst. The existence of secondary mesoporous systems may influence the location and state of the active Mo species, simultaneously lead to easier access to the active sites for reactants, and better diffusion of aromatics products, thus improving the activities of the catalysts. It can be concluded that

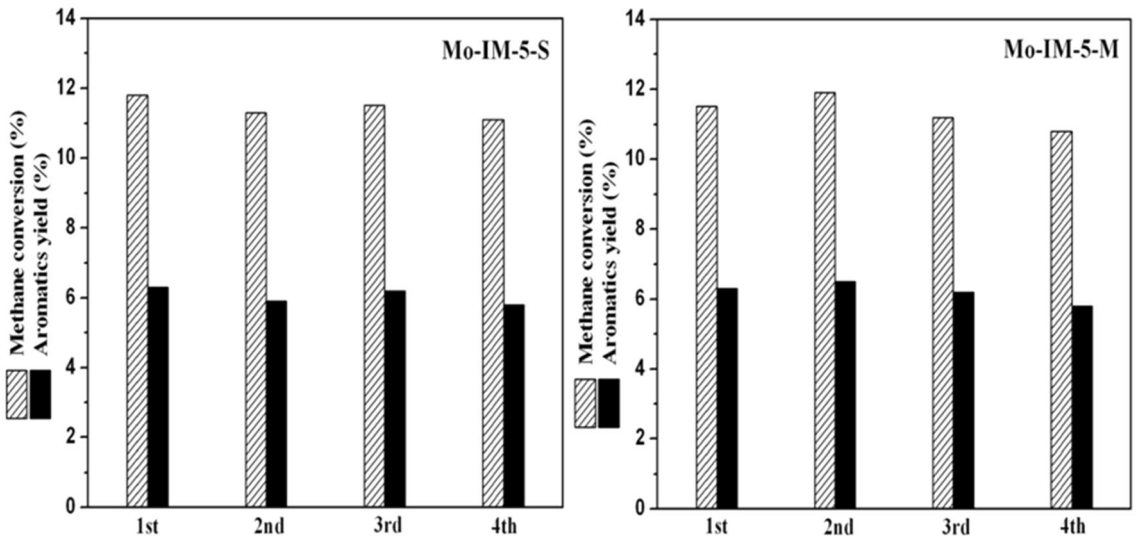

Fig. 7 The comparison of the catalytic performances over Mo-IM-5-S and Mo-IM-5-M catalysts for four successive runs. Reaction condition: $T = 973$ K, 1 atm, GHSV = 1500/h; reaction time: 60 min

appropriate secondary mesoporous system in IM-5 zeolite is favorable for enhancing catalytic behavior of the catalyst in the non-oxidative aromatization of methane.

Acknowledgements This work was supported by the Youth Fund of Changchun University of Science and Technology (XJJLG-2015-12).

References

1. Lunsford JH (2000) Catalytic conversion of methane to more useful chemicals and fuels: a challenge for the 21st century. Catal Today 63:165–174
2. Wang L, Tao L, Xie M, Xu G (1993) Dehydrogenation and aromatization of methane under non-oxidizing conditions. Catal Lett 21:35–41
3. Wang D, Kan Q, Xu N, Wu P, Wu T (2004) Study on methane aromatization over MoO_3/HMCM-49 catalyst. Catal Today 93:75–80
4. Liu H, Hu J, Li Z, Wu S, Liu L, Guan J, Kan Q (2013) Synthesis of zeolite IM-5 under rotating and static conditions and the catalytic performance of Mo/H-IM-5 catalyst in methane non-oxidative aromatization. Kinet Catal 54:443–450
5. Xu C, Guan J, Wu S, Jia M, Wu T, Kan Q (2010) Catalytic performance of zeolite ITQ-13 with 9- and 10-member rings for methane dehydroaromation. React Kinet Mech Catal 99:193–199
6. Liu H, Yang S, Wu S, Shang F, Yu X, Xu C, Guan J, Kan Q (2011) Synthesis of Mo/TNU-9 (TNU-9 Taejon National University No. 9) catalyst and its catalytic performance in methane non-oxidative aromatization. Energy 36:1582–1589
7. Liu B, Zhang Y, Liu J, Tian M, Zhang F, Au CT, Cheung ASC (2011) Characteristic and mechanism of methane dehydroaromatization over Zn-Based/HZSM-5 catalysts under conditions of atmospheric pressure and supersonic jet expansion. J Phys Chem C 115:16954–16962
8. Kusmiyati Amin NAS (2005) Dual effects of supported W catalysts for dehydroaromatization of methane in the absence of oxygen. Catal Lett 102:69–78
9. Tan P, Au CT, Lai SY (2006) Methane dehydrogenation and aromatization over 4 wt% Mn/HZSM-5 in the absence of an oxidant. Catal Lett 112:239–245
10. Luzgin MV, Gabrienko AA, Rogov VA, Toktarev AV, Parmon VN, Stepanov AG (2010) The "alkyl" and "carbenium" pathways of methane activation on Ga-modified zeolite BEA: 13C solid-state NMR and GC-MS study of methane aromatization in the presence of higher alkane. J Phys Chem C 114:21555–21561
11. Weckhuysen BM, Rosynek MP, Lunsford JH (1998) Characterization of surface carbon formed during the conversion of methane to benzene over Mo/H-ZSM-5 catalysts. Catal Lett 52:31–36
12. Ma D, Wang D, Su L, Shu Y, Xu Y, Bao X (2002) Carbonaceous deposition on Mo/HMCM-22 catalysts for methane aromatization: a TP technique investigation. J Catal 208:260–269
13. Wu P, Kan Q, Wang X, Wang D, Xing H, Yang P, Wu T (2005) Acidity and catalytic properties for methane conversion of Mo/HZSM-5 catalyst modified by reacting with organometallic complex. Appl Catal A 282:39–44
14. Liu S, Dong Q, Ohnishi R, Ichikawa M (1997) Remarkable non-oxidative conversion of methane to naphthalene and benzene on Co and Fe modified Mo/HZSM-5 catalysts. Chem Commun 15:1455–1456
15. Ma S, Guo X, Zhao L, Scottc S, Bao X (2013) Recent progress in methane dehydroaromatization: from laboratory curiosities to promising technology. J Energy Chem 22:1–20
16. Xu Y, Wang J, Suzuki Y, Zhang Z (2011) Effect of transition metal additives on the catalytic stability of Mo/HZSM-5 in the methane dehydroaromatization under periodic CH_4–H_2 switch operation at 1073 K. Appl Catal A 409–410:181–193
17. Guo X, Fang G, Li G, Ma H, Fan H, Yu L, Ma C, Wu X, Deng D, Wei M, Tan D, Si R, Zhang S, Li J, Sun L, Tang Z, Pan X, Bao X (2014) Direct, nonoxidative conversion of methane to ethylene, aromatics, and hydrogen. Science 344:616–619
18. Corma A, Chica A, Guil JM, Llopis FJ, Mabilon G, Perdigón-Melón JA, Valencia S (2000) Determination of the pore topology of zeolite IM-5 by means of catalytic test reactions and hydrocarbon adsorption measurements. J Catal 189:382–394
19. Corma A, Mengual J, Miguel PJ (2013) IM-5 zeolite for steam catalytic cracking of naphtha to produce propene and ethene. An alternative to ZSM-5 zeolite. Appl Catal A 460–461:106–115
20. Vennestrøm PNR, Janssens TVW, Kustov A, Grill M, Puig-Molina A, Lundegaard LF, Tiruvalam RR, Concepción P, Corma A (2014) Influence of lattice stability on hydrothermal deactivation of Cu-ZSM-5 and Cu-IM-5 zeolites for selective catalytic reduction of NO_x by NH_3. J Catal 309:477–490
21. Liu H, Wu S, Guo Y, Shang F, Yu X, Ma Y, Xu C, Guan J, Kan Q (2011) Synthesis of Mo/IM-5 catalyst and its catalytic behavior in methane non-oxidative aromatization. Fuel 90:1515–1521
22. Chu N, Yang J, Li C, Cui J, Zhao Q, Yin X, Lu J, Wang J (2009) An unusual hierarchical ZSM-5 microsphere with good catalytic performance in methane dehydroaromatization. Microporous Mesoporous Mater 118:169–175
23. Chu N, Wang J, Zhang Y, Yang J, Lu J, Yin D (2010) Nestlike hollow hierarchical MCM-22 microspheres: synthesis and exceptional catalytic properties. Chem Mater 22:2757–2763
24. Hu J, Wu S, Liu H, Ding H, Li Z, Guan J, Kan Q (2014) Effect of mesopore structure of TNU-9 on methane dehydroaromatization. RSC Adv 4:26577–26584
25. Liu H, Yang S, Hu J, Shang F, Li Z, Xu C, Guan J, Kan Q (2012) A comparison study of mesoporous Mo/H-ZSM-5 and conventional Mo/H-ZSM-5 catalysts in methane non-oxidative aromatization. Fuel Process Technol 96:195–202
26. Zhao D, Feng J, Huo Q, Melosh N, Fredrickson GH, Chmelka BF, Stucky GD (1998) Triblock copolymer syntheses of mesoporous silica with periodic 50 to 300 angstrom pores. Science 279:548–552
27. Beck J, Vartuli J, Roth W, Leonowicz M, Kresge C, Schmitt K, Chu CTW, Olson DH, Sheppard EW (1992) A new family of mesoporous molecular sieves prepared with liquid crystal templates. J Am Chem Soc 114:10834–10843
28. Li B, Li S, Li N, Chen H, Zhang W, Bao X, Lin B (2006) Structure and acidity of Mo/ZSM-5 synthesized by solid state reaction for methane dehydrogenation and aromatization. Microporous Mesoporous Mater 88:244–253